First Constraints on Light Sterile Neutrino Oscillations from Combined Appearance and Disappearance Searches with the MicroBooNE Detector

Louis, William Charles III
Gollapinni, Sowjanya
Ross-Lonergan, Mark Paul
Fine, Robert Duncan
Oza, Nupur Parag
Hicks, R

Los Alamos
NATIONAL LABORATORY

NNSA
National Nuclear Security Administration

First Constraints on Light Sterile Neutrino Oscillations from Combined Appearance and Disappearance Searches with the MicroBooNE Detector

P. Abratenko,[34] D. Andrade Aldana,[14] J. Anthony,[4] L. Arellano,[19] J. Asaadi,[33] A. Ashkenazi,[31] S. Balasubramanian,[11] B. Baller,[11] G. Barr,[24] J. Barrow,[20,31] V. Basque,[11] L. Bathe-Peters,[13] O. Benevides Rodrigues,[30] S. Berkman,[11] A. Bhanderi,[19] M. Bhattacharya,[11] M. Bishai,[2] A. Blake,[16] B. Bogart,[21] T. Bolton,[15] J. Y. Book,[13] L. Camilleri,[9] D. Caratelli,[3] I. Caro Terrazas,[8] F. Cavanna,[11] G. Cerati,[11] Y. Chen,[27] J. M. Conrad,[20] M. Convery,[27] L. Cooper-Troendle,[37] J. I. Crespo-Anadón,[5] M. Del Tutto,[11] S. R. Dennis,[4] P. Detje,[4] A. Devitt,[16] R. Diurba,[1] R. Dorrill,[14] K. Duffy,[24] S. Dytman,[25] B. Eberly,[29] A. Ereditato,[1] J. J. Evans,[19] R. Fine,[17] O. G. Finnerud,[19] W. Foreman,[14] B. T. Fleming,[37] N. Foppiani,[13] D. Franco,[37] A. P. Furmanski,[22] D. Garcia-Gamez,[12] S. Gardiner,[11] G. Ge,[9] S. Gollapinni,[32,17] O. Goodwin,[19] E. Gramellini,[11] P. Green,[19] H. Greenlee,[11] W. Gu,[2] R. Guenette,[19] P. Guzowski,[19] L. Hagaman,[37] O. Hen,[20] R. Hicks,[17] C. Hilgenberg,[22] G. A. Horton-Smith,[15] B. Irwin,[22] R. Itay,[27] C. James,[11] X. Ji,[2] L. Jiang,[35] J. H. Jo,[37] R. A. Johnson,[7] Y.-J. Jwa,[9] D. Kalra,[9] N. Kamp,[20] G. Karagiorgi,[9] W. Ketchum,[11] M. Kirby,[11] T. Kobilarcik,[11] I. Kreslo,[1] M. B. Leibovitch,[3] I. Lepetic,[26] J.-Y. Li,[10] K. Li,[37] Y. Li,[2] K. Lin,[26] B. R. Littlejohn,[14] W. C. Louis,[17] X. Luo,[3] K. Manivannan,[30] C. Mariani,[35] D. Marsden,[19] J. Marshall,[36] N. Martinez,[15] D. A. Martinez Caicedo,[28] K. Mason,[34] A. Mastbaum,[26] N. McConkey,[19] V. Meddage,[15] K. Miller,[6] J. Mills,[34] A. Mogan,[8] T. Mohayai,[11] M. Mooney,[8] A. F. Moor,[4] C. D. Moore,[11] L. Mora Lepin,[19] J. Mousseau,[21] S. Mulleriababu,[1] D. Naples,[25] A. Navrer-Agasson,[19] N. Nayak,[2] M. Nebot-Guinot,[10] J. Nowak,[16] M. Nunes,[30] N. Oza,[17] O. Palamara,[11] N. Pallat,[22] V. Paolone,[25] A. Papadopoulou,[20] V. Papavassiliou,[23] H. B. Parkinson,[10] S. F. Pate,[23] N. Patel,[16] Z. Pavlovic,[11] E. Piasetzky,[31] I. D. Ponce-Pinto,[37] I. Pophale,[16] S. Prince,[13] X. Qian,[2] J. L. Raaf,[11] V. Radeka,[2] M. Reggiani-Guzzo,[19] L. Ren,[23] L. Rochester,[27] J. Rodriguez Rondon,[28] M. Rosenberg,[34] M. Ross-Lonergan,[17] C. Rudolf von Rohr,[1] G. Scanavini,[37] D. W. Schmitz,[6] A. Schukraft,[11] W. Seligman,[9] M. H. Shaevitz,[9] R. Sharankova,[11] J. Shi,[4] A. Smith,[4] E. L. Snider,[11] M. Soderberg,[30] S. Söldner-Rembold,[19] J. Spitz,[21] M. Stancari,[11] J. St. John,[11] T. Strauss,[11] S. Sword-Fehlberg,[23] A. M. Szelc,[10] W. Tang,[32] N. Taniuchi,[4] K. Terao,[27] C. Thorpe,[16] D. Torbunov,[2] D. Totani,[3] M. Toups,[11] Y.-T. Tsai,[27] J. Tyler,[15] M. A. Uchida,[4] T. Usher,[27] B. Viren,[2] M. Weber,[1] H. Wei,[18] A. J. White,[37] Z. Williams,[33] S. Wolbers,[11] T. Wongjirad,[34] M. Wospakrik,[11] K. Wresilo,[4] N. Wright,[20] W. Wu,[11] E. Yandel,[3] T. Yang,[11] L. E. Yates,[11] H. W. Yu,[2] G. P. Zeller,[11] J. Zennamo,[11] and C. Zhang[2]

(MicroBooNE Collaboration)*

[1]Universität Bern, Bern CH-3012, Switzerland
[2]Brookhaven National Laboratory (BNL), Upton, New York 11973, USA
[3]University of California, Santa Barbara, California 93106, USA
[4]University of Cambridge, Cambridge CB3 0HE, United Kingdom
[5]Centro de Investigaciones Energéticas, Medioambientales y Tecnológicas (CIEMAT), Madrid E-28040, Spain
[6]University of Chicago, Chicago, Illinois 60637, USA
[7]University of Cincinnati, Cincinnati, Ohio 45221, USA
[8]Colorado State University, Fort Collins, Colorado 80523, USA
[9]Columbia University, New York, New York 10027, USA
[10]University of Edinburgh, Edinburgh EH9 3FD, United Kingdom
[11]Fermi National Accelerator Laboratory (FNAL), Batavia, Illinois 60510, USA
[12]Universidad de Granada, Granada E-18071, Spain
[13]Harvard University, Cambridge, Massachusetts 02138, USA
[14]Illinois Institute of Technology (IIT), Chicago, Illinois 60616, USA
[15]Kansas State University (KSU), Manhattan, Kansas 66506, USA
[16]Lancaster University, Lancaster LA1 4YW, United Kingdom
[17]Los Alamos National Laboratory (LANL), Los Alamos, New Mexico 87545, USA
[18]Louisiana State University, Baton Rouge, Louisiana 70803, USA
[19]The University of Manchester, Manchester M13 9PL, United Kingdom
[20]Massachusetts Institute of Technology (MIT), Cambridge, Massachusetts 02139, USA
[21]University of Michigan, Ann Arbor, Michigan 48109, USA
[22]University of Minnesota, Minneapolis, Minnesota 55455, USA
[23]New Mexico State University (NMSU), Las Cruces, New Mexico 88003, USA
[24]University of Oxford, Oxford OX1 3RH, United Kingdom

^{25}University of Pittsburgh, Pittsburgh, Pennsylvania 15260, USA
^{26}Rutgers University, Piscataway, New Jersey 08854, USA
^{27}SLAC National Accelerator Laboratory, Menlo Park, California 94025, USA
^{28}South Dakota School of Mines and Technology (SDSMT), Rapid City, South Dakota 57701, USA
^{29}University of Southern Maine, Portland, Maine 04104, USA
^{30}Syracuse University, Syracuse, New York 13244, USA
^{31}Tel Aviv University, Tel Aviv, Israel, 69978
^{32}University of Tennessee, Knoxville, Tennessee 37996, USA
^{33}University of Texas, Arlington, Texas 76019, USA
^{34}Tufts University, Medford, Massachusetts 02155, USA
^{35}Center for Neutrino Physics, Virginia Tech, Blacksburg, Virginia 24061, USA
^{36}University of Warwick, Coventry CV4 7AL, United Kingdom
^{37}Wright Laboratory, Department of Physics, Yale University, New Haven, Connecticut 06520, USA

We present a search for eV-scale sterile neutrino oscillations in the MicroBooNE liquid argon detector, simultaneously considering all possible appearance and disappearance effects within the $3+1$ active-to-sterile neutrino oscillation framework. We analyze the neutrino candidate events for the recent measurements of charged-current ν_e and ν_μ interactions in the MicroBooNE detector, using data corresponding to an exposure of 6.37×10^{20} protons on target from the Fermilab booster neutrino beam. We observe no evidence of light sterile neutrino oscillations and derive exclusion contours at the 95% confidence level in the plane of the mass-squared splitting Δm^2_{41} and the sterile neutrino mixing angles $\theta_{\mu e}$ and θ_{ee}, excluding part of the parameter space allowed by experimental anomalies. Cancellation of ν_e appearance and ν_e disappearance effects due to the full $3+1$ treatment of the analysis leads to a degeneracy when determining the oscillation parameters, which is discussed in this Letter and will be addressed by future analyses.

The discoveries of solar [1] and atmospheric neutrino oscillations [2] have motivated a broad experimental program dedicated to studying neutrino mixing. While most measurements [3–13] are consistent with three-flavor (3ν) neutrino oscillations as described by the Pontecorvo-Maki-Nakagawa-Sakata (PMNS) formalism [14–16], several experimental anomalies [17–27] can possibly be explained by a hypothetical sterile neutrino with a mass at the eV scale [15,28]. The SAGE [17] and GALLEX [18] experiments, and more recently, the BEST [19,20] experiment, have observed lower than expected ν_e rates from radioactive sources, which is known as the gallium anomaly. Reactor neutrino experiments have measured lower $\bar{\nu}_e$ rates [21] than the expectation based on reactor antineutrino flux calculations [22,23]. This observation is referred to as the reactor anomaly. An oscillation signal in the reactor $\bar{\nu}_e$ energy spectrum over distances of a few meters was reported by the Neutrino-4 [24] Collaboration. In addition to these observed $\overset{(-)}{\nu}_e$ deficits, excesses of

$\overset{(-)}{\nu}_e$-like events were also observed in some $\overset{(-)}{\nu}_\mu$ dominated accelerator neutrino experiments. The LSND Collaboration [25] observed an anomalous excess of $\bar{\nu}_e$-like events, and the MiniBooNE Collaboration [26,27] observed an excess of low-energy electronlike events.

These anomalies are in strong tension with other experimental results within the $3(\text{active}) + 1(\text{sterile})$ oscillation framework as seen in a global fit of the data [29]. In addition, recent experimental measurements [30,31] and improvements of the reactor antineutrino flux calculation [32,33] lead to a plausible resolution of the reactor antineutrino anomaly. The Neutrino-4 anomaly is largely excluded by the results from other very short baseline reactor neutrino experiments, for example, PROSPECT [34], STEREO [35], DANSS [36], NEOS [37], although it is consistent with the gallium anomaly.

The MicroBooNE Collaboration has recently reported a first set of searches related to the MiniBooNE low-energy excess, targeting multiple final-state topologies of the charged-current (CC) ν_e interactions [38–41] and the neutral-current (NC) Δ resonance decay that produces a single photon in the final state [42]. The MicroBooNE detector [43] has a similar location and is exposed to the same booster neutrino beam (BNB) [44] as the MiniBooNE detector. Utilizing the liquid argon time projection chamber (LArTPC) technology that can provide good

e/γ separation, MicroBooNE has achieved high-performance ν_e selections and observes no evidence of a ν_e excess [38–41]. These results disfavor the hypothesis that the MiniBooNE low-energy excess originates solely from an excess of ν_e interactions. Instead, one or more additional mechanisms [45–52] are required to explain the MiniBooNE observations.

A light sterile neutrino would profoundly impact fundamental physics. In addition to testing models that may explain both the MicroBooNE and MiniBooNE low-energy ν_e observations, interpreting the MicroBooNE ν_e results in the context of a sterile neutrino can provide valuable statements beyond the conclusions already reached by the current analyses, and examine the remaining experimental anomalies that may be explained by a sterile neutrino. Recent phenomenological studies have examined the MicroBooNE ν_e results in the context of a sterile neutrino hypothesis. One study [53] considers a ν_e disappearance-only hypothesis, while another [54] considers the full $3 + 1$ oscillation effect.

In this Letter, we present a new analysis testing the sterile neutrino hypothesis in a full $3 + 1$ oscillation framework with detailed event-level information. We use the dataset from the MicroBooNE inclusive ν_e CC measurement [41], and compare the results to the parameter space allowed by the LSND, gallium (including BEST), and Neutrino-4 anomalies. We simultaneously consider short-baseline sterile-neutrino-induced ν_e appearance and ν_e disappearance. This treatment can lead to cancellations that result in a degeneracy when determining the oscillation parameters, which we will introduce in more detail in this Letter.

The MicroBooNE detector [43] is a 10.4 m long, 2.6 m wide, and 2.3 m tall LArTPC, located on-axis of the BNB at Fermilab. It consists of about 85 metric tons of liquid argon in the TPC active volume for ionization charge detection along with an array of photomultiplier tubes [55] for scintillation light detection. It sits at a distance of 468.5 m from the target of the BNB, which uses protons with a kinetic energy of 8 GeV impinging on the target, producing secondary hadrons. The hadrons are mostly pions or kaons that decay in flight, producing a neutrino beam through their decay. The MicroBooNE BNB dataset was collected entirely in neutrino mode and consists of a very pure ν_μ beam with a small $\bar{\nu}_\mu$ contamination and a ν_e contamination of $< 1\%$.

We perform a full $3 + 1$ (4ν) neutrino oscillation analysis, capitalizing on the seven channels of ν_e and ν_μ selections and their statistical and systematic uncertainties from the MicroBooNE inclusive ν_e low-energy excess search [41]. The analysis uses the BNB Runs 1–3 dataset with an exposure of 6.369×10^{20} protons on target (POT). In addition to the standard Monte Carlo (MC) samples for intrinsic ν_e and ν_μ events in the BNB, a dedicated $\nu_\mu \rightarrow \nu_e$ oscillation sample was generated to appropriately take into account the flux and cross-section systematic uncertainties

related to the ν_e appearance events. The seven channels comprise fully contained (FC) and partially contained (PC) ν_e CC processes, FC and PC ν_μ CC processes without final-state π^0 mesons, FC and PC ν_μ CC processes with final-state π^0 mesons, and a NC channel with final-state π^0 mesons. The fully contained events are defined as those that have all reconstructed TPC activity (i.e., charge depositions) within a fiducial volume 3 cm from the TPC boundaries. Because there are ν_μ and ν_e components in the BNB flux, the ν_e appearance (from ν_μ), ν_e disappearance, and ν_μ disappearance oscillation effects in the $3 + 1$ framework are simultaneously applied to the predicted signal and background events in *all* seven channels in the oscillation fit. The ν_μ appearance effect is neglected because of the very low fraction of intrinsic ν_e in the BNB flux. This strategy takes full advantage of the statistics of the selected ν_e and ν_μ events in the FC and PC channels, and at the same time maintains the capability to apply data constraints across channels through a joint fit to the seven channels, thereby reducing the systematic uncertainty in the oscillation analysis. The neutrino energy reconstruction primarily follows a calorimetric method with an energy resolution of approximately 10%–15% and a bias of 5%–10% for CC events [41]. In the reconstruction of NC events, we use this method to estimate the energy transfer with an invisible outgoing neutrino. The reconstruction of visible energy for the NC events in this analysis has a similar bias and energy resolution to the neutrino energy reconstruction of CC events.

We use an extended 4×4 unitary PMNS matrix (U) to describe the $3 + 1$ neutrino mixing between the flavor and mass eigenstates. Following the common parameterization [29,56], the elements of U relevant to this Letter can be expressed as

$$
\begin{aligned}
|U_{e4}|^2 &= \sin^2\theta_{14}, \\
|U_{\mu 4}|^2 &= \cos^2\theta_{14}\sin^2\theta_{24}, \\
|U_{s4}|^2 &= \cos^2\theta_{14}\cos^2\theta_{24}\cos^2\theta_{34},
\end{aligned} \tag{1}
$$

where s denotes the sterile neutrino flavor. Given the energy range of the neutrino flux at MicroBooNE, in the parameter space with $\Delta m_{41}^2 \gg |\Delta m_{31}^2|$, the short-baseline oscillation probability from α-flavor to β-flavor neutrinos in vacuum approximates to

$$
P_{\nu_\alpha \rightarrow \nu_\beta} = \delta_{\alpha\beta} + (-1)^{\delta_{\alpha\beta}}\sin^2 2\theta_{\alpha\beta}\sin^2\Delta_{41}, \tag{2}
$$

where $\delta_{\alpha\beta}$ is the Kronecker delta,

$$
\Delta_{41} \equiv \frac{\Delta m_{41}^2 L}{4E} = 1.267\left(\frac{\Delta m_{41}^2}{\text{eV}^2}\right)\left(\frac{\text{MeV}}{E}\right)\left(\frac{L}{m}\right), \tag{3}
$$

and

$$\sin^2 2\theta_{\alpha\beta} = 4|U_{\alpha4}|^2|\delta_{\alpha\beta} - |U_{\beta4}|^2|. \quad (4)$$

We define $\theta_{\alpha\beta}$ as the effective mixing angles, which can be expressed as

$$\sin^2 2\theta_{ee} = \sin^2 2\theta_{14},$$
$$\sin^2 2\theta_{\mu e} = \sin^2 2\theta_{14}\sin^2\theta_{24},$$
$$\sin^2 2\theta_{\mu\mu} = 4\cos^2\theta_{14}\sin^2\theta_{24}(1 - \cos^2\theta_{14}\sin^2\theta_{24}),$$
$$\sin^2 2\theta_{es} = \sin^2 2\theta_{14}\cos^2\theta_{24}\cos^2\theta_{34},$$
$$\sin^2 2\theta_{\mu s} = \cos^4\theta_{14}\sin^2 2\theta_{24}\cos^2\theta_{34}. \quad (5)$$

Ignoring the oscillation effect in the negligible neutrino background outside of the detector cryostat, for the other CC and NC signal or background events in all seven channels, we use $\sin^2 2\theta_{ee}$ and $\sin^2 2\theta_{\mu e}$ to predict the ν_e CC energy spectrum, $\sin^2 2\theta_{\mu\mu}$ to predict the ν_μ CC energy spectrum, and $\sin^2 2\theta_{es}$ and $\sin^2 2\theta_{\mu s}$ to predict the NC energy spectrum. We fix θ_{34} to 0 ($\cos^2\theta_{34} = 1$) since it has a negligible impact in this analysis given the current contribution of the NC events in the seven channels. The NC events are mainly used to constrain the NC π^0 background in the ν_e CC channels and the NC event disappearance can be probed in the future with a more inclusive NC selection. As a result, the three oscillation parameters Δm_{41}^2, $\sin^2\theta_{14}$, and $\sin^2\theta_{24}$ are free to vary in the fit.

It is important to note that in an oscillation analysis such as this one, performed in a ν_μ-dominated beam with a non-negligible intrinsic ν_e component, the effects of ν_e disappearance and appearance can lead to a cancellation effect on the impact on the expected event rates. Equation (6) demonstrates this quantitatively,

$$N_{\nu_e}(E_\nu) = T_{\nu_e}(E_\nu)[1 + (R(E_\nu) \times \sin^2\theta_{24} - 1)$$
$$\times \sin^2 2\theta_{14}\sin^2\Delta_{41}(E_\nu)], \quad (6)$$

where T_{ν_e} is the number of intrinsic ν_e in the flux, and R is the ratio between the number of intrinsic ν_μ and ν_e for a given true neutrino energy E_ν. When $\sin^2\theta_{24}$ approaches the inverse of the average value of $R(E_\nu)$ in the BNB, i.e., $1/R \approx 0.005$, the ν_e appearance and ν_e disappearance contributions mostly cancel leading to a diminished oscillation effect in the ν_e channels, independent of the values of Δm_{41}^2 and $\sin^2\theta_{14}$. This results in a decreased sensitivity to sterile neutrino oscillations in this specific parameter space, which was not fully considered in some experimental results [25–27].

The test statistic used in the oscillation fit is the combined-Neyman-Pearson (CNP) χ^2 [57]

$$\chi^2 = (M - P)^T \cdot (\text{Cov}_{\text{stat}} + \text{Cov}_{\text{syst}})^{-1} \cdot (M - P), \quad (7)$$

where M and P are vectors of the measurements and the predictions for the seven channels, respectively, Cov_{stat} is the CNP-format statistical uncertainty covariance matrix corresponding to $3/(1/M_i + 2/P_i)$ for the ith bin, and Cov_{syst} is the covariance matrix of the full systematic uncertainty. The systematic uncertainties are estimated from (i) the neutrino flux prediction of the BNB [58], (ii) ν-argon cross section modeling from the GENIE event generator [59,60], (iii) final-state hadron-argon interactions in the GEANT4 simulation [61,62], (iv) residual discrepancies in detector response after calibrations [63–66], and (v) finite statistics of the MC samples used for central value predictions. An additional uncertainty is conservatively determined for the events that originate from the neutrino interactions outside the LArTPC cryostat. The covariance matrices Cov_{stat} and Cov_{syst} depend on the prediction for the central values in each energy bin and thus vary as a function of the oscillation parameters in the fit.

The data is found to agree with the 3ν (null) hypothesis within 1 standard deviation (σ) significance. The joint fit to the seven channels yields a best-fit result of $\Delta m_{41}^2 = 1.295$ eV^2, $\sin^2\theta_{14} = 0.936$, and $\sin^2\theta_{24} = 0$ with a χ^2 of 86.62 for 179 degrees of freedom. The best-fit values give $\sin^2 2\theta_{ee} = 0.240$ and $\sin^2 2\theta_{\mu e(\mu\mu)} = 0$, and the corresponding predicted ν_e energy spectra are shown in Fig. 1. The energy distributions of the other channels can be found in the Supplemental Material [67]. In this oscillation fit, the χ^2 value is largely symmetric relative to $\sin^2\theta_{14} = 0.5$ because the dominant oscillation effects from ν_e appearance and ν_e disappearance depend on $\sin^2 2\theta_{14}$. The best-fit slightly prefers $\sin^2\theta_{14} = 0.936$ to $\sin^2\theta_{14} = 0.064$. We obtain a $\Delta\chi_{\text{data}}^2 = \chi_{\text{null},3\nu}^2 - \chi_{\text{min},4\nu}^2 = 2.53$ with 3 degrees of freedom, corresponding to a p value of 0.426 following the Feldman-Cousins (F-C) procedure [76]. The Supplemental Material [67] presents the F-C $\Delta\chi^2$ distribution corresponding to the null hypothesis. It also provides the values of $\Delta\chi_{\text{data}}^2 = \chi_{4\nu}^2 - \chi_{\text{min},4\nu}^2$ for each 4ν hypothesis in an $80 \times 60 \times 60$ three-dimensional grid of the oscillation parameters spanning over 0.01–100 eV^2 in Δm_{41}^2, 0.0001–1.0 in $\sin^2\theta_{14}$, and 0.0001–1.0 in $\sin^2\theta_{24}$ on a logarithmic scale.

Since the data are found to be consistent with the 3ν hypothesis, exclusion limits are calculated using the frequentist-motivated CL$_s$ method [77], which is commonly used for the discovery or exclusion limits in neutrino oscillation analyses [34–36,68]. The CL$_s$ test statistic is based on $\Delta\chi_{\text{CL}_s}^2 = \chi_{4\nu}^2 - \chi_{3\nu}^2$, which compares the null 3ν hypothesis and an alternative 4ν hypothesis. It is defined by

$$\text{CL}_s = \frac{1 - p_{4\nu}}{1 - p_{3\nu}}, \quad (8)$$

where $p_{4\nu}$ ($p_{3\nu}$) is the p value of $\Delta\chi_{\text{CL}_s,\text{data}}^2$ assuming the 4ν (null 3ν) hypothesis is true. The p value is determined in a
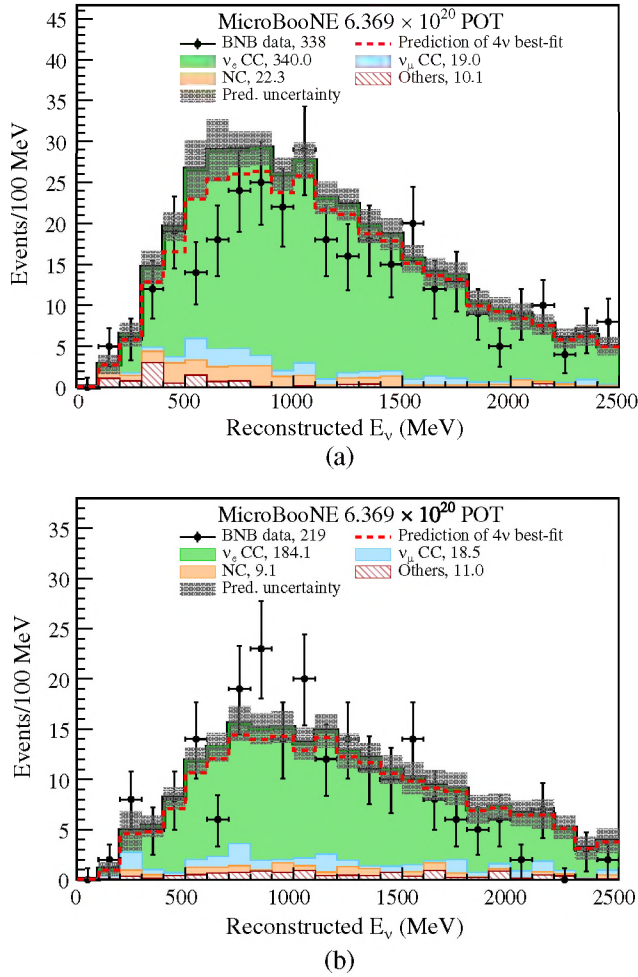
(a)

(b)

FIG. 1. Reconstructed neutrino energy of (a) fully contained ν_e CC and (b) partially contained ν_e CC events. The data points are shown with statistical error bars. The MC predictions of the 3ν hypothesis for ν_e CC events (green) and different types of backgrounds are shown in the stack of histograms. The category "Others" corresponds to the background events originating from either beam neutrino interactions outside the fiducial volume or cosmic-ray muons. The dashed red histogram represents the MC prediction of the 4ν best-fit with $\Delta m_{41}^2 = 1.295$ eV^2, $\sin^2\theta_{14} = 0.936$ ($\sin^2 2\theta_{ee} = 0.240$), and $\sin^2\theta_{24} = 0$ ($\sin^2 2\theta_{\mu e(\mu\mu)} = 0$). The MC predictions and shaded error bands correspond to the central values and systematic uncertainties for each energy bin with constraints (Sec. VI A in Ref. [41]) from the ν_μ CC and π^0 channels as used in the joint fit to the seven channels.

frequentist approach by throwing pseudoexperiments following the corresponding full covariance matrix assuming a hypothesis is true. The region with CL$_s \leq 1 - \alpha$ is excluded at the confidence level (C.L.) of α.

Figure 2 shows the frequentist CL$_s$ exclusion contours and sensitivities at the 95% C.L. in the (Δm_{41}^2, $\sin^2 2\theta_{\mu e}$) plane and in the (Δm_{41}^2, $\sin^2 2\theta_{ee}$) plane. Since there are three free oscillation parameters in the fit, the exclusion limit in any two-dimensional (2D) parameter space is

obtained by profiling the third dimension. After profiling, the exclusion limit corresponds to the value of the third dimension that gives the minimal $\chi_{4\nu}^2$ along that dimension at each point in the 2D parameter space. This procedure is a natural choice according to Refs. [78–80]. The $\sin^2\theta_{24}$ value after profiling in this analysis is generally small, between 0 and 0.01, which is consistent with the existing experimental constraints [29,81,82]. All sensitivities in this Letter are calculated using the Asimov dataset [83] from MC simulation, corresponding to the 3ν central value predictions without oscillation.

The Asimov sensitivities in the scenarios with only ν_e appearance or only ν_e disappearance are often quoted in the literature [25–27,84,85] as an approximation, neglecting the oscillation effects from the intrinsic ν_e or ν_μ component in the beam. These approximations result in overly optimistic sensitivities compared to the 2D profiled results because the cancellation between ν_e appearance and ν_e disappearance is neglected. Our primary result, therefore, does not use this approximation, but we include data exclusion limits taking only ν_e appearance or only ν_e disappearance into account in the Supplemental Material [67] in order to compare to historical results.

The ν_e disappearance-only case corresponds to $\sin^2\theta_{24} = 0$. However, ν_e appearance only is a valid approximation *only* when the intrinsic ν_e disappearance effect is small compared to the ν_e appearance effect since nonzero ν_e appearance requires both nonzero ν_e and ν_μ disappearances. As seen in Fig. 2(a), the ν_e appearance-only sensitivity asymptotically converges with the 2D profiled sensitivity in the low Δm_{41}^2 (< 0.2 eV^2) region, where the effect of ν_e disappearance becomes negligible compared to the ν_e appearance effect.

The LSND allowed region shown in Fig. 2(a) was calculated using the ν_e appearance-only approximation. After considering ν_e disappearance, it will move towards larger $\sin^2 2\theta_{\mu e}$ by a small amount because the intrinsic $\bar{\nu}_e$ contribution is small compared to the observed excess of $\bar{\nu}_e$-like events in the LSND experiment. Part of the LSND-allowed region is excluded by the MicroBooNE 2D profiled result, especially in the high and low Δm_{41}^2 regions. Portions of the allowed regions of the Neutrino-4 and gallium anomalies in Fig. 2(b) are within the MicroBooNE data exclusion limit, with part of the region between $\Delta m_{41}^2 = 3$ and 10 eV^2 excluded. Other experimental constraints on the related sterile neutrino parameter space can be found in the Supplemental Material [67].

The MicroBooNE results shown in this Letter are predominantly limited by the impact of the degeneracy caused by ν_e appearance and ν_e disappearance effects on the event rate. Future analysis strategies can break this degeneracy, further improving the sensitivity reach of a $3 + 1$ sterile neutrino search. The degeneracy can be addressed leveraging that MicroBooNE detects neutrinos from both the BNB and NuMI beam lines. In addition to
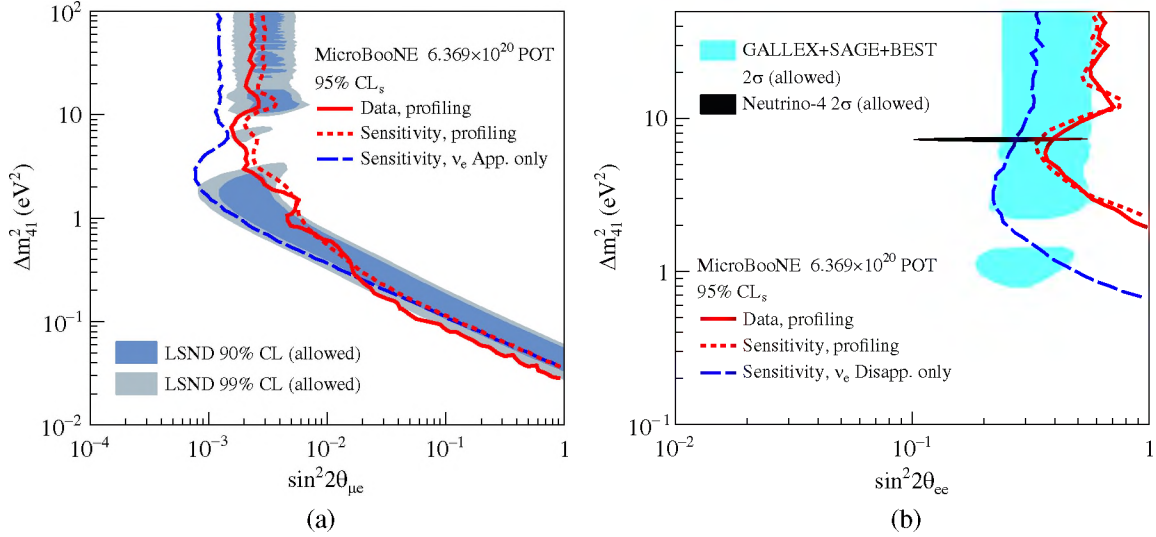
FIG. 2. MicroBooNE CL_s exclusion contours at the 95% C.L. in the plane of Δm_{41}^2 and (a) $\sin^2 2\theta_{\mu e}$ or (b) $\sin^2 2\theta_{ee}$. The red solid (dashed) curve represents the MicroBooNE 95% CL_s data exclusion (Asimov sensitivity) limits after profiling over the mixing angle $\sin^2 \theta_{24}$. The blue long-dashed curve represents the MicroBooNE 95% CL_s Asimov sensitivity in the scenario of (a) ν_e appearance only or (b) ν_e disappearance only as opposed to the full $3 + 1$ oscillation result. In (a), the LSND 90% and 99% C.L. allowed regions [25] using the ν_e appearance-only approximation are shown as the light blue and gray shaded areas, respectively. In (b), the cyan shaded area represents the 2σ allowed region of the gallium anomaly from the experimental results of GALLEX, SAGE, and BEST [20]. The 2σ allowed region of the Neutrino-4 experiment [24] is also shown in (b).

BNB, the MicroBooNE detector is situated at 680 m from the NuMI target and 8° off axis from the NuMI beam direction, where NuMI is the neutrino beam from the main injector [86]. It uses protons with a kinetic energy of 120 GeV, much higher than BNB, impinging on the target. The ratios of the ν_e to the ν_μ fluxes are 0.005 and 0.04 for the BNB and NuMI beams, respectively. The cancellation of ν_e disappearance and ν_e appearance effects therefore proceeds differently for the two beams, breaking the degeneracy that would be observed in an experiment with a single beam line. Multidetector oscillation analyses will also help break the degeneracy in some regions because the overall cancellation effect depends on not only the $R(E_\nu)$ term but also the oscillation term as a function of the ratio L/E. Such a multiple-detector strategy, as adopted by the short-baseline neutrino program (SBN) [87], will further improve the capability to probe the sterile neutrino parameter space with substantially reduced neutrino cross-section and flux uncertainties.

In summary, the MicroBooNE BNB Run 1–3 data show no evidence of sterile neutrino oscillations and are found to be consistent with the 3ν hypothesis within 1σ significance. The current exclusion contours, corresponding to a BNB exposure of 6.369×10^{20} POT, allow for a test of part of the sterile neutrino parameter space suggested by other experimental anomalies. This result provides the first constraints, competitive in the relatively high Δm_{41}^2 region, on the eV-scale sterile neutrino parameter space measured in a LArTPC detector from an accelerator neutrino source. This Letter paves the way for future neutrino oscillation

searches with LArTPCs in the SBN and DUNE [88] experiments. An upcoming search for sterile neutrino oscillations at MicroBooNE combining the BNB and NuMI data will improve upon the current result by breaking the parameter degeneracy in some regions and by using data from two different beam lines.

*microboone_info@fnal.gov

[1] Q. R. Ahmad *et al.* (SNO Collaboration), Measurement of the rate of $\nu_e + d \to p + p + e^-$ interactions produced by ^{8}B solar neutrinos at the Sudbury Neutrino Observatory, Phys. Rev. Lett. **87**, 071301 (2001).

[2] Y. Fukuda *et al.* (Super-Kamiokande Collaboration), Evidence for Oscillation of Atmospheric Neutrinos, Phys. Rev. Lett. **81**, 1562 (1998).

[3] B. Aharmim *et al.* (SNO Collaboration), Combined analysis of all three phases of solar neutrino data from the Sudbury Neutrino Observatory, Phys. Rev. C **88**, 025501 (2013).

[4] K. Abe *et al.* (Super-Kamiokande Collaboration), Atmospheric neutrino oscillation analysis with external constraints in Super-Kamiokande I-IV, Phys. Rev. D **97**, 072001 (2018).

[5] M. G. Aartsen *et al.* (IceCube Collaboration), Measurement of Atmospheric Neutrino Oscillations at 6–56 GeV with IceCube DeepCore, Phys. Rev. Lett. **120**, 071801 (2018).

[6] A. Gando *et al.* (KamLAND Collaboration), Reactor on-off antineutrino measurement with KamLAND, Phys. Rev. D **88**, 033001 (2013).

[7] D. Adey *et al.* (Daya Bay Collaboration), Measurement of the Electron Antineutrino Oscillation with 1958 Days of Operation at Daya Bay, Phys. Rev. Lett. **121**, 241805 (2018).

[8] G. Bak *et al.* (RENO Collaboration), Measurement of Reactor Antineutrino Oscillation Amplitude and Frequency at RENO, Phys. Rev. Lett. **121**, 201801 (2018).

[9] Y. Abe *et al.* (Double Chooz Collaboration), Measurement of θ_{13} in Double Chooz using neutron captures on hydrogen with novel background rejection techniques, J. High Energy Phys. 01 (2016) 163.

[10] K. Abe *et al.* (T2K Collaboration), Improved constraints on neutrino mixing from the T2K experiment with 3.13×10^{21} protons on target, Phys. Rev. D **103**, 112008 (2021).

[11] M. A. Acero *et al.* (NOvA Collaboration), Improved measurement of neutrino oscillation parameters by the NOvA experiment, Phys. Rev. D **106**, 032004 (2022).

[12] P. Adamson *et al.* (MINOS+ Collaboration), Precision Constraints for Three-Flavor Neutrino Oscillations from the Full MINOS+ and MINOS Dataset, Phys. Rev. Lett. **125**, 131802 (2020).

[13] N. Agafonova *et al.* (OPERA Collaboration), Final Results of the OPERA Experiment on ν_τ Appearance in the CNGS Neutrino Beam, Phys. Rev. Lett. **120**, 211801 (2018); **121**, 139901(E) (2018).

[14] B. Pontecorvo, Mesonium and anti-mesonium, Sov. Phys. JETP **6**, 429 (1957), http://jetp.ras.ru/cgi-bin/dn/e_006_02_0429.pdf.

[15] B. Pontecorvo, Neutrino experiments and the problem of conservation of leptonic charge, Sov. Phys. JETP **26**, 984 (1968), http://jetp.ras.ru/cgi-bin/dn/e_026_05_0984.pdf.

[16] Z. Maki, M. Nakagawa, and S. Sakata, Remarks on the unified model of elementary particles, Prog. Theor. Phys. **28**, 870 (1962).

[17] J. N. Abdurashitov *et al.* (SAGE Collaboration), Measurement of the solar neutrino capture rate with gallium metal. III: Results for the 2002–2007 data-taking period, Phys. Rev. C **80**, 015807 (2009).

[18] F. Kaether, W. Hampel, G. Heusser, J. Kiko, and T. Kirsten, Reanalysis of the GALLEX solar neutrino flux and source experiments, Phys. Lett. B **685**, 47 (2010).

[19] V. V. Barinov, S. N. Danshin, V. N. Gavrin, V. V. Gorbachev, D. S. Gorbunov *et al.*, Search for electron-neutrino transitions to sterile states in the BEST experiment, Phys. Rev. C **105**, 065502 (2022).

[20] V. V. Barinov *et al.*, Results from the Baksan Experiment on Sterile Transitions (BEST), Phys. Rev. Lett. **128**, 232501 (2022).

[21] G. Mention, M. Fechner, T. Lasserre, T. A. Mueller, D. Lhuillier, M. Cribier, and A. Letourneau, Reactor antineutrino anomaly, Phys. Rev. D **83**, 073006 (2011).

[22] T. A. Mueller *et al.*, Improved predictions of reactor antineutrino spectra, Phys. Rev. C **83**, 054615 (2011).

[23] P. Huber, Determination of antineutrino spectra from nuclear reactors, Phys. Rev. C **84**, 024617 (2011); **85**, 029901 (E) (2012).

[24] A. P. Serebrov *et al.*, Search for sterile neutrinos with the Neutrino-4 experiment and measurement results, Phys. Rev. D **104**, 032003 (2021).

[25] A. Aguilar-Arevalo *et al.* (LSND Collaboration), Evidence for neutrino oscillations from the observation of $\bar{\nu}_e$ appearance in a $\bar{\nu}_\mu$ beam, Phys. Rev. D **64**, 112007 (2001).

[26] A. A. Aguilar-Arevalo *et al.* (MiniBooNE Collaboration), Improved Search for $\bar{\nu}_\mu \to \bar{\nu}_e$ Oscillations in the MiniBooNE Experiment, Phys. Rev. Lett. **110**, 161801 (2013).

[27] A. A. Aguilar-Arevalo *et al.* (MiniBooNE Collaboration), Updated MiniBooNE neutrino oscillation results with increased data and new background studies, Phys. Rev. D **103**, 052002 (2021).

[28] K. N. Abazajian *et al.*, Light sterile neutrinos: A white paper, arXiv:1204.5379.

[29] C. Giunti and T. Lasserre, eV-scale sterile neutrinos, Annu. Rev. Nucl. Part. Sci. **69**, 163 (2019).

[30] F. P. An *et al.* (Daya Bay Collaboration), Evolution of the Reactor Antineutrino Flux and Spectrum at Daya Bay, Phys. Rev. Lett. **118**, 251801 (2017).

[31] F. P. An *et al.* (Daya Bay Collaboration), Antineutrino energy spectrum unfolding based on the Daya Bay measurement and its applications, Chin. Phys. C **45**, 073001 (2021).

[32] V. Kopeikin, M. Skorokhvatov, and O. Titov, Reevaluating reactor antineutrino spectra with new measurements of the ratio between ^{235}U and ^{239}Pu β spectra, Phys. Rev. D **104**, L071301 (2021).

[33] C. Giunti, Y. F. Li, C. A. Ternes, and Z. Xin, Reactor antineutrino anomaly in light of recent flux model refinements, Phys. Lett. B **829**, 137054 (2022).

[34] M. Andriamirado *et al.* (PROSPECT Collaboration), Improved short-baseline neutrino oscillation search and

energy spectrum measurement with the PROSPECT experiment at HFIR, Phys. Rev. D **103**, 032001 (2021).

[35] H. Almazán *et al.* (STEREO Collaboration), Improved sterile neutrino constraints from the STEREO experiment with 179 days of reactor-on data, Phys. Rev. D **102**, 052002 (2020).

[36] M. Danilov and N. Skrobova (DANSS Collaboration), New results from the DANSS experiment, Proc. Sci., EPS-HEP2021 (**2022**) 241 [arXiv:2112.13413].

[37] Z. Atif *et al.* (RENO, NEOS Collaborations), Search for sterile neutrino oscillations using RENO and NEOS data, Phys. Rev. D **105**, L111101 (2022).

[38] P. Abratenko *et al.* (MicroBooNE Collaboration), Search for an Excess of Electron Neutrino Interactions in MicroBooNE Using Multiple Final-State Topologies, Phys. Rev. Lett. **128**, 241801 (2022).

[39] P. Abratenko *et al.* (MicroBooNE Collaboration), Search for an anomalous excess of charged-current quasielastic ν_e interactions with the MicroBooNE experiment using Deep-Learning-based reconstruction, Phys. Rev. D **105**, 112003 (2022).

[40] P. Abratenko *et al.* (MicroBooNE Collaboration), Search for an anomalous excess of charged-current ν_e interactions without pions in the final state with the MicroBooNE experiment, Phys. Rev. D **105**, 112004 (2022).

[41] P. Abratenko *et al.* (MicroBooNE Collaboration), Search for an anomalous excess of inclusive charged-current ν_e interactions in the MicroBooNE experiment using e reconstruction, Phys. Rev. D **105**, 112005 (2022).

[42] P. Abratenko *et al.* (MicroBooNE Collaboration), Search for Neutrino-Induced Neutral-Current Δ Radiative Decay in MicroBooNE and a First Test of the MiniBooNE Low Energy Excess under a Single-Photon Hypothesis, Phys. Rev. Lett. **128**, 111801 (2022).

[43] R. Acciarri *et al.* (MicroBooNE Collaboration), Design and construction of the MicroBooNE detector, J. Instrum. **12**, P02017 (2017).

[44] I. Stancu *et al.*, Technical design report for the 8 GeV beam, Report No. FERMILAB-DESIGN-2001-03, 10.2172/1212167 (2001).

[45] A. de Gouvêa, O. L. G. Peres, S. Prakash, and G. V. Stenico, On the decaying-sterile-neutrino solution to the electron (anti)neutrino appearance anomalies, J. High Energy Phys. 07 (2020) 141.

[46] S. Vergani, N. W. Kamp, A. Diaz, C. A. Argüelles, J. M. Conrad, M. H. Shaevitz, and M. A. Uchida, Explaining the MiniBooNE excess through a mixed model of neutrino oscillation and decay, Phys. Rev. D **104**, 095005 (2021).

[47] J. Asaadi, E. Church, R. Guenette, B. J. P. Jones, and A. M. Szelc, New light Higgs boson and short-baseline neutrino anomalies, Phys. Rev. D **97**, 075021 (2018).

[48] D. S. M. Alves, W. C. Louis, and P. G. deNiverville, Quasi-sterile neutrinos from dark sectors. Part I. BSM matter effects in neutrino oscillations and the short-baseline anomalies, J. High Energy Phys. 08 (2022) 034.

[49] E. Bertuzzo, S. Jana, P. A. N. Machado, and R. Zukanovich Funchal, Dark Neutrino Portal to Explain MiniBooNE excess, Phys. Rev. Lett. **121**, 241801 (2018).

[50] P. Ballett, S. Pascoli, and M. Ross-Lonergan, U(1)' mediated decays of heavy sterile neutrinos in MiniBooNE, Phys. Rev. D **99**, 071701(R) (2019).

[51] W. Abdallah, R. Gandhi, and S. Roy, Two-Higgs doublet solution to the LSND, MiniBooNE and muon $g-2$ anomalies, Phys. Rev. D **104**, 055028 (2021).

[52] W. Abdallah, R. Gandhi, and S. Roy, Understanding the MiniBooNE and the muon and electron $g-2$ anomalies with a light Z' and a second Higgs doublet, J. High Energy Phys. 12 (2020) 188.

[53] P. B. Denton, Sterile Neutrino Search with MicroBooNE's Electron Neutrino Disappearance Data, Phys. Rev. Lett. **129**, 061801 (2022).

[54] C. A. Argüelles, I. Esteban, M. Hostert, K. J. Kelly, J. Kopp, P. A. N. Machado, I. Martinez-Soler, and Y. F. Perez-Gonzalez, MicroBooNE and the ν_e Interpretation of the MiniBooNE Low-Energy Excess, Phys. Rev. Lett. **128**, 241802 (2022).

[55] T. Briese *et al.*, Testing of cryogenic photomultiplier tubes for the MicroBooNE experiment, J. Instrum. **8**, T07005 (2013).

[56] H. Harari and M. Leurer, Recommending a standard choice of Cabibbo angles and KM phases for any number of generations, Phys. Lett. B **181**, 123 (1986).

[57] X. Ji, W. Gu, X. Qian, H. Wei, and C. Zhang, Combined Neyman–Pearson chi-square: An improved approximation to the Poisson-likelihood chi-square, Nucl. Instrum. Methods Phys. Res., Sect. A **961**, 163677 (2020).

[58] A. A. Aguilar-Arevalo *et al.* (MiniBooNE Collaboration), Neutrino flux prediction at MiniBooNE, Phys. Rev. D **79**, 072002 (2009).

[59] L. Alvarez-Ruso *et al.* (GENIE Collaboration), Recent highlights from GENIE v3, Eur. Phys. J. Special Topics **230**, 4449 (2021).

[60] P. Abratenko *et al.* (MicroBooNE Collaboration), New $CC0\pi$ GENIE model tune for MicroBooNE, Phys. Rev. D **105**, 072001 (2022).

[61] S. Agostinelli *et al.* (GEANT4 Collaboration), GEANT4–a simulation toolkit, Nucl. Instrum. Methods Phys. Res., Sect. A **506**, 250 (2003).

[62] J. Calcutt, C. Thorpe, K. Mahn, and L. Fields, Geant4Reweight: A framework for evaluating and propagating hadronic interaction uncertainties in Geant4, J. Instrum. **16**, P08042 (2021).

[63] C. Adams *et al.* (MicroBooNE Collaboration), A method to determine the electric field of liquid argon time projection chambers using a UV laser system and its application in MicroBooNE, J. Instrum. **15**, P07010 (2020).

[64] C. Adams *et al.* (MicroBooNE Collaboration), Calibration of the charge and energy loss per unit length of the MicroBooNE liquid argon time projection chamber using muons and protons, J. Instrum. **15**, P03022 (2020).

[65] P. Abratenko *et al.* (MicroBooNE Collaboration), Measurement of space charge effects in the MicroBooNE LArTPC using cosmic muons, J. Instrum. **15**, P12037 (2020).

[66] P. Abratenko *et al.* (MicroBooNE Collaboration), Novel approach for evaluating detector-related uncertainties in a LArTPC using MicroBooNE data, Eur. Phys. J. C **82**, 454 (2022).

[67] See Supplemental Material at http://link.aps.org/supplemental/10.1103/PhysRevLett.130.011801 for $\Delta\chi^2_{\text{data}}$ values in the 3D parameter space, additional data exclusion limits, and other experimental results, which includes Refs. [20,24,25,34,37,41,68–75].

[68] P. Adamson *et al.* (MINOS+, Daya Bay Collaborations), Improved Constraints on Sterile Neutrino Mixing from Disappearance Searches in the MINOS, MINOS+, Daya Bay, and Bugey-3 Experiments, Phys. Rev. Lett. **125,** 071801 (2020).

[69] P. Astier *et al.* (NOMAD Collaboration), Search for $\nu_\mu \to \nu_e$ oscillations in the NOMAD experiment, Phys. Lett. B **570,** 19 (2003).

[70] B. Armbruster *et al.* (KARMEN Collaboration), Upper limits for neutrino oscillations $\bar{\nu}_\mu \to \bar{\nu}_e$ from muon decay at rest, Phys. Rev. D **65,** 112001 (2002).

[71] M. Aker *et al.* (KATRIN Collaboration), Improved eV-scale sterile-neutrino constraints from the second KATRIN measurement campaign, Phys. Rev. D **105,** 072004 (2022).

[72] H. Almazán *et al.* (STEREO Collaboration), Interpreting reactor antineutrino anomalies with STEREO data, arXiv:2210.07664.

[73] M. Danilov, New results from the DANSS experiment, Proc. Sci., ICHEP2022 (**2022**) 616 [arXiv:2211.01208].

[74] C. Giunti, Y. F. Li, C. A. Ternes, and Y. Y. Zhang, Neutrino-4 anomaly: Oscillations or fluctuations?, Phys. Lett. B **816,** 136214 (2021).

[75] A. A. Aguilar-Arevalo *et al.* (MiniBooNE Collaboration), MiniBooNE and MicroBooNE Combined Fit to a 3 + 1 Sterile Neutrino Scenario, Phys. Rev. Lett. **129,** 201801 (2022).

[76] G. J. Feldman and R. D. Cousins, Unified approach to the classical statistical analysis of small signals, Phys. Rev. D **57,** 3873 (1998).

[77] A. L. Read, Presentation of search results: The CL(s) technique, J. Phys. G **28,** 2693 (2002).

[78] C.-S. Chuang and T. L. Lai, Hybrid resampling methods for confidence intervals, Statistica Sinica **10,** 1 (2000), https://www3.stat.sinica.edu.tw/statistica/j10n1/j10n11/j10n11.htm.

[79] B. Sen, M. Walker, and M. Woodroofe, On the unified method with nuisance parameters, Statistica Sinica **19,** 301 (2009), https://www3.stat.sinica.edu.tw/statistica/J19N1/j19n116/j19n116.html.

[80] M. A. Acero *et al.* (NOvA Collaboration), The Profiled Feldman-Cousins technique for confidence interval construction in the presence of nuisance parameters, arXiv:2207.14353.

[81] P. Adamson *et al.* (MINOS+ Collaboration), Search for Sterile Neutrinos in MINOS and MINOS+ using a Two-Detector Fit, Phys. Rev. Lett. **122,** 091803 (2019).

[82] M. G. Aartsen *et al.* (IceCube Collaboration), eV-Scale Sterile Neutrino Search Using Eight Years of Atmospheric Muon Neutrino Data from the IceCube Neutrino Observatory, Phys. Rev. Lett. **125,** 141801 (2020).

[83] G. Cowan, K. Cranmer, E. Gross, and O. Vitells, Asymptotic formulae for likelihood-based tests of new physics, Eur. Phys. J. C **71,** 1554 (2011); **73,** 2501(E) (2013).

[84] K. Abe *et al.* (T2K Collaboration), Search for short baseline ν_e disappearance with the T2K near detector, Phys. Rev. D **91,** 051102 (2015).

[85] B. Abi *et al.* (DUNE Collaboration), Prospects for beyond the Standard Model physics searches at the Deep Underground Neutrino Experiment, Eur. Phys. J. C **81,** 322 (2021).

[86] P. Adamson *et al.*, The NuMI Neutrino Beam, Nucl. Instrum. Methods Phys. Res., Sect. A **806,** 279 (2016).

[87] P. A. Machado, O. Palamara, and D. W. Schmitz, The short-baseline neutrino program at Fermilab, Annu. Rev. Nucl. Part. Sci. **69,** 363 (2019).

[88] B. Abi *et al.* (DUNE Collaboration), Long-baseline neutrino oscillation physics potential of the DUNE experiment, Eur. Phys. J. C **80,** 978 (2020).